

ACCEPTED MANUSCRIPT

# Monte Carlo calculation of the TG-43 dosimetry parameters for the INTRABEAM source with spherical applicators

To cite this article before publication: David Santiago Ayala Alvarez *et al* 2021 *Phys. Med. Biol.* in press <https://doi.org/10.1088/1361-6560/ac309f>

## Manuscript version: Accepted Manuscript

Accepted Manuscript is “the version of the article accepted for publication including all changes made as a result of the peer review process, and which may also include the addition to the article by IOP Publishing of a header, an article ID, a cover sheet and/or an ‘Accepted Manuscript’ watermark, but excluding any other editing, typesetting or other changes made by IOP Publishing and/or its licensors”

This Accepted Manuscript is © 2021 Institute of Physics and Engineering in Medicine.

During the embargo period (the 12 month period from the publication of the Version of Record of this article), the Accepted Manuscript is fully protected by copyright and cannot be reused or reposted elsewhere.

As the Version of Record of this article is going to be / has been published on a subscription basis, this Accepted Manuscript is available for reuse under a CC BY-NC-ND 3.0 licence after the 12 month embargo period.

After the embargo period, everyone is permitted to use copy and redistribute this article for non-commercial purposes only, provided that they adhere to all the terms of the licence <https://creativecommons.org/licenses/by-nc-nd/3.0>

Although reasonable endeavours have been taken to obtain all necessary permissions from third parties to include their copyrighted content within this article, their full citation and copyright line may not be present in this Accepted Manuscript version. Before using any content from this article, please refer to the Version of Record on IOPscience once published for full citation and copyright details, as permissions will likely be required. All third party content is fully copyright protected, unless specifically stated otherwise in the figure caption in the Version of Record.

View the [article online](#) for updates and enhancements.

# Monte Carlo calculation of the TG-43 dosimetry parameters for the INTRABEAM source with spherical applicators

David Santiago Ayala Alvarez, Peter G F Watson, Marija Popovic, Veng Jean Heng, Michael D C Evans and Jan Seuntjens

Medical Physics Unit, McGill University and Cedars Cancer Center, Montreal, Canada

E-mail: david.ayalaalvarez@mail.mcgill.ca

**Abstract.** The relative TG-43 dosimetry parameters of the INTRABEAM (Carl Zeiss Meditec AG, Jena, Germany) bare probe were recently reported by Ayala Alvarez et al. (2020). The current study focuses on the dosimetry characterization of the INTRABEAM source with the eight available spherical applicators according to the TG-43 formalism using Monte Carlo (MC) simulations. This report includes the calculated dose-rate conversion coefficients that determine the absolute dose rate to water at a reference point of 10 mm from the applicator surface, based on calibration air-kerma rate measurements at 50 cm from the source on its transverse plane. Since the air-kerma rate measurements are not yet provided from a standards laboratory for the INTRABEAM, the values in the present study were calculated with MC. This approach is aligned with other works in the search for standardization of the dosimetry of electronic brachytherapy sources. As a validation of the MC model, depth dose calculations along the source axis were compared with calibration data from the source manufacturer. The calculated dose-rate conversion coefficients were 434.0 for the bare probe, and 683.5, 548.3, 449.9, 376.5, 251.0, 225.6, 202.8, and 182.6 for the source with applicators of increasing diameter from 15 to 50 mm, respectively. The radial dose and the 2D anisotropy functions of the TG-43 formalism were also obtained and tabulated in this document. This work presents the data required by a treatment planning system for the characterization of the INTRABEAM system in the context of intraoperative radiotherapy applications.

*Keywords:* electronic brachytherapy, brachytherapy dosimetry, TG-43, Monte Carlo, INTRABEAM.

## 1. Introduction

During the last two decades, the INTRABEAM system (Carl Zeiss Meditec AG, Jena, Germany) and the Xofigo Axxent<sup>®</sup> (iCAD, Inc. Nashua, NH) have been the most utilized electronic brachytherapy (eBT) sources (Nath et al. 2016). The INTRABEAM has been

*TG-43 parameters for the INTRABEAM source with spherical applicators* 2

extensively used for breast intraoperative radiotherapy (IORT), with TARGIT trials as some of the best known published clinical trials (Vaidya et al. 2014). Clinical trials are still underway to show impact of INTRABEAM IORT in the setting of brain irradiation of glioblastoma multiforme surgical cavity (Giordano et al. 2014, Giordano et al. 2018).

The INTRABEAM system features a miniature electron accelerator where low-energy x-ray photons are produced after the electrons strike a gold target. The INTRABEAM source is used with clinical applicators that vary in shape and size, depending on clinical application. Spherical INTRABEAM applicators are most widely used in IORT settings. They are available in different sizes ranging in diameter from 15 to 50 mm in steps of 5 mm (described by Eaton (2012)).

In current clinical practice, the dosimetry of the INTRABEAM relies on calibration depth dose data provided by the manufacturer. The calibration curves for the bare source probe are measured in water along the probe axis. In addition, depth-specific transfer functions are provided, and they convert bare probe data to depth dose curves for each applicator. Independent dosimetry methods for the INTRABEAM that are feasible in the clinical workflow have been proposed but a consensus dosimetry protocol, with traceability to a primary standards dosimetry laboratory (PSDL), is yet to be developed. In this context, the National Institute of Standards and Technology (NIST) initiated a new primary standard to be applied to eBT sources (Seltzer et al. 2014). The NIST standard has been used to calibrate the Xofig Axxent source (Hiatt et al. 2016) based on a modification of the American Association of Physicists in Medicine (AAPM) Task Group No. 43 Report (TG-43) (Nath et al. 1995) and its updated version (TG-43U1) (Rivard et al. 2004). With this variation, the absorbed dose at a reference point in water is obtained from the air-kerma rate measured at 50 cm from the source axis in a PSDL using a dose-rate conversion coefficient (DeWerd et al. 2015). Well chambers have been accepted and calibrated as transfer instruments that permit the transfer of air-kerma rate measurements to secondary calibration facilities, making the standards viable for clinical use (Seltzer et al. 2014, DeWerd et al. 2015). Currently, there is no accepted air-kerma-based primary standard for the INTRABEAM system. In parallel to the NIST research, an approach in terms of absorbed dose to water has been developed at the National Metrology Institute of Germany (PTB) (Schneider et al. 2016). With this method, the dose to water at a reference depth of 10 mm, along the source axis, is obtained from calibration air-kerma measurements at reference conditions. Abudra'A et al. (2020) reported the results of the PTB standard evaluated in the INTRABEAM system with a spherical applicator of 40 mm diameter. A different approach has been developed by Watson et al. (2017, 2018, 2019) in which a depth-dependent Monte Carlo (MC) calculated factor,  $C_Q$ , converts air-kerma rates obtained with an air-kerma calibrated ionization chamber (PTW 34013) to absorbed dose to water.

During the IORT workflow with INTRABEAM, treatment times and dose to critical structures are determined based on the tabulated calibration data, the prescription dose, and the distance from applicator surface (Carl Zeiss Meditec AG 2011, Culberson et al. 2020). This approach provides a 1D dose distribution and assumes isotropic

### *TG-43 parameters for the INTRABEAM source with spherical applicators*

dose falloff. However, accurate 3D dose distributions accounting for the source polar anisotropy are required in order to assess the relative dose contributions of IORT and complementary techniques. In this context, Shamsabadi et al. (2020) have modeled the INTRABEAM source with spherical applicators using GEANT4 and evaluated the polar anisotropy in dose distribution at 10 mm from the applicators' surface. They have also assessed the impact of such applicators on the spectral and dosimetric characteristics of the x-ray beam. A convenient alternative for 3D dose calculations with eBT sources would be to explore their similarity to radionuclide brachytherapy sources and characterize the eBT source according to the AAPM TG-43 protocol. TG-43-based treatment planning systems (TPS) are fast and available in most clinics offering brachytherapy with radionuclides. The TG-43 formalism was previously used to characterize the Xofigo source (Rivard et al. 2006, Hiatt et al. 2015). For the INTRABEAM, relative TG-43 parameters were recently reported for the bare probe (Ayala Alvarez et al. 2020).

The aim of this work is to characterize the INTRABEAM source with spherical applicators according to the TG-43 formalism using MC simulations. A complete set of TG-43 data of the INTRABEAM will permit 3D dose distribution calculations within the treatment planning framework that exists for brachytherapy with radionuclides. Moreover, it will provide a means of assessing cumulative dose distributions of IORT and external beam radiotherapy on patient's 3D images.

## **2. Materials and Methods**

### *2.1. INTRABEAM source and spherical applicators*

The INTRABEAM system contains a miniature x-ray source where electrons are accelerated towards a 0.5  $\mu\text{m}$  thick gold target situated on the inner surface of an evacuated 100 mm long, 3.2 mm outer diameter needle (Dinsmore et al. 1996, Yanch & Harte 1996). The electron source spectrum exhibits a Gaussian distribution of energy centered at 50 keV and full width at half maximum (FWHM) of 5 keV (Clausen et al. 2012). Following the interaction of electrons with the target, x-rays are produced by fluorescence and bremsstrahlung. Clinical use of the system is usually carried out with a nominal 50 kV tube voltage and a current of 40  $\mu\text{A}$ . A MC model of the INTRABEAM source probe was previously developed and validated by Watson et al. (2017, 2018, 2019), and the relative TG-43 parameters for the system's bare probe were obtained (Ayala Alvarez et al. 2020). In this work, the specifications for source geometry and materials were reproduced using the egs++ library (Kawrakow et al. 2009) of EGSnrc. The electron beam was modeled as two concentric rings of radii 0.6 to 0.7 mm and 0.7 to 0.8 mm, with weighting factors of 1.05 and 1.55, respectively (Clausen et al. 2012).

MC simulations of the dose distributions in water using the INTRABEAM system with spherical applicators were performed. These applicators were placed on the

*TG-43 parameters for the INTRABEAM source with spherical applicators*

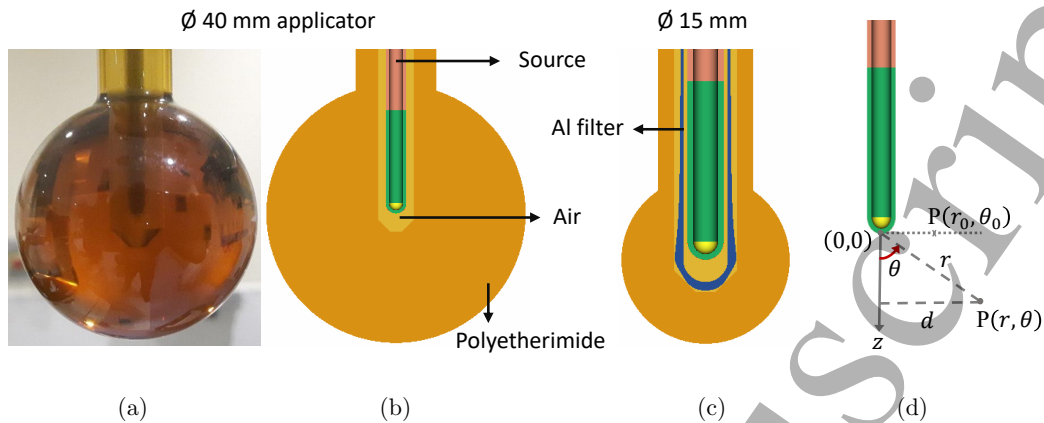


**Figure 1.** Rendering of the spherical applicators models for the MC simulations. In (a), a picture of the 40 mm diameter applicator is compared with its simulation geometry shown in (b). In (c), the 15 mm applicator rendering is presented as an example of the smallest applicators, with sphere diameters from 15 to 30 mm, which include an aluminium filter. (d) shows the reference coordinate system used for determining the TG-43 parameters for the INTRABEAM source.

INTRABEAM source with the source tip at the sphere center. The bulk material of the applicators is a biocompatible polyetherimide called ULTEM (Carl Zeiss Meditec AG 2017) with a nominal mass density of  $1.27 \text{ g/cm}^3$ . The smallest applicators with diameters of 15 to 30 mm include an aluminium (Al) filter to provide a degree of beam hardening by preferentially absorbing low-energy photons. Simulated applicator geometries with their materials are shown in figure figure 1(b) for a 40 mm diameter applicator, and in (c) for the smallest 15 mm diameter applicator. Detailed dimensions and material compositions were provided by Zeiss and are proprietary. The water phantom and annular scoring volumes were the same as presented by Ayala Alvarez et al. (2020) for simulations of the bare probe. The dose distribution was obtained outside the applicator volume and partial volume effects in voxels at the applicator surface were corrected following the procedure described by Clausen et al. (2012).

## 2.2. Radiation transport parameters

Monte Carlo simulations were performed using `egs_brachy` (v2017.09.15) (Chamberland et al. 2016) from the EGSnrc code system. The range of the secondary electrons produced by low-energy photons is generally small compared to macroscopic millimeter-sized voxels. For instance, the range of the secondary electrons produced by the INTRABEAM photon spectrum in water would be of around  $1.8 \times 10^{-3} \text{ cm}$  (Beaulieu et al. 2012), which is near two orders of magnitude smaller than the minimum linear dimension of the scoring voxels used in this study (1 mm). Therefore, dose to water was approximated as water electronic kerma obtained via a tracklength estimator, resulting in reduced computation times. The computation of kerma with `egs_brachy` makes use of

### TG-43 parameters for the INTRABEAM source with spherical applicators 5

precalculated mass energy-absorption coefficients for water ( $\rho = 1.0 \text{ g cm}^{-3}$ ) provided as a separate file in the EGSnrc code system. Simulations were run in two stages for each spherical applicator. In the first stage,  $1 \times 10^8$  starting electrons were transported from the ring-shaped electron beam inside the probe, and a phase space was scored at the applicator surface with data of the particles energy, position, velocity, charge and statistical weight. In the second stage, particles were run from the phase space generated for each applicator, and doses were scored in 0.4 mm thick annular water voxels centered at the source axis. On average,  $7.8 \times 10^8$  histories were run in the second stage, depending on the number of particles stored in the phase space file for each applicator. A list of the physics processes and transport parameters is presented in table 1, following the recommendations of the AAPM TG-268 (Sechopoulos et al. 2018) for the reporting of MC studies. As variance reduction techniques, bremsstrahlung cross-sections were enhanced in the gold target by a factor of 50, and bremsstrahlung events were split by a factor of 100 during the first stage of the simulations.

#### 2.3. TG-43 parameters

Relative TG-43 parameters have been previously reported for the Xofig Axxent source (Hiatt et al. 2015) and the INTRABEAM bare probe (Ayala Alvarez et al. 2020). For both sources the effective focal spot is small and the point-source approximation was used to model the geometry function,  $G_P(r, \theta)$ . With this assumption, the geometry function obeys the inverse square law of the distance from the source. With the TG-43 formalism, the measured air-kerma strength,  $S_K$ , required a conversion of the air-kerma rate to *in-vacuo* conditions by applying corrections for scatter and attenuation in air and in the surrounding media. However, this procedure was not appropriate for eBT sources, since the scatter and attenuation corrections were significant. For example, the attenuation correction for the Xofig source was higher than 25% (DeWerd et al. 2015). For this reason, a modified formalism using the air-kerma rate measured in air, instead of air-kerma strength, was developed at the National Institute of Standards and Technology (NIST) (Seltzer et al. 2014). Based on the air-kerma rate standard, DeWerd et al. (2015) proposed a modified formalism to calculate the dose rate in water according to

$$\dot{D}_i(r, \theta) = \dot{K}_{50\text{cm}} \chi_i(10 \text{ mm}, \pi/2) G_P(r, \theta) g_i(r) F_i(r, \theta), \quad (1)$$

where the subscript  $i$  makes reference to the dose rate calculation using an applicator  $i$ ,  $\dot{K}_{50\text{cm}}$  is the air-kerma rate measured in air at 50 cm from the source axis on the transverse plane at the source tip level, with traceability to a PSDL,  $\chi_i$  is called the dose-rate conversion coefficient at the reference point in water ( $r_0 = 10 \text{ mm}$  from applicator surface and  $\theta_0 = 90^\circ$ ),  $G_P(r, \theta) = 1/r^2$  is the geometry function with point-source approximation, and  $g_i(r)$  and  $F_i(r, \theta)$  are the radial dose function and the 2D anisotropy function for the applicator  $i$ , respectively. The dose-rate conversion coefficient,  $\chi_i$ , was calculated as

$$\chi_i(10 \text{ mm}, \pi/2) = \left( \frac{\dot{K}_{50\text{cm}}}{\dot{D}_i(10 \text{ mm}, \pi/2)} \right), \quad (2)$$

TG-43 parameters for the INTRABEAM source with spherical applicators 6

**Table 1.** Summary of the characteristics of the MC method used to obtain the TG-43 parameters.

Item	Description	References
Code	EGSnrc 2019 egs++ library, EGSnrc 2019 master branch egs_brachy (v2017.09.15)	Kawrakow & Rogers (2019) Kawrakow et al. (2009) Chamberland et al. (2016)
Validation	The MC model was validated by comparison of computed depth dose profiles along the source axis with the calibration data provided by the manufacturer (Carl Zeiss AG)	
Timing	Time required to obtain each applicator phase space: $\sim 10$ h with a cluster of 124 cores split in five nodes of Intel(R) Xeon(R) CPU models: two E5-2697 v3 @ 2.60 GHz, two E5-2687W @ 3.10 GHz and one Gold 6140 @ 2.30 GHz. The time required to obtain the dose distribution in water from the phase space for each applicator was $\sim 100$ h	
Source description	Two stages: <b>1.</b> Divergent electron beam hitting the target in the shape of two concentric rings with a Gaussian distribution of energy centered at 50 keV with a FWHM of 5 keV. <b>2.</b> Phase-space data stored at each applicator surface	Clausen et al. (2012)
Cross-sections	Photoelectric and Rayleigh scattering: XCOM Compton: relativistic impulse approximation Bremsstrahlung: NRC Electron impact ionization: PENELOPE Atomic relaxations with explicit M and N-shell transitions: EADL	Berger et al. (2010) Kawrakow & Rogers (2019) Kawrakow & Rogers (2019) Bote & Salvat (2008) Watson & Seuntjens (2016)
Transport parameters	Boundary crossing algorithm: Exact PCUT = 1 keV, ECUT inside the source = 512 keV. Electrons were not transported outside the source (ECUT = 1 MeV)	Kawrakow & Rogers (2019)
Variance reduction techniques	Bremsstrahlung and photon cross-section enhancement, uniform bremsstrahlung splitting	Chamberland et al. (2016)
Scored quantities	Absorbed dose to water (collision kerma approximation)	
# histories /statistical uncertainty	For $\dot{D}_i(10\text{ mm}, \pi/2)$ : $1 \times 10^8$ original particles/0.03% uncertainty, in average for all applicators	
Statistical methods	History-by-history	Chamberland et al. (2016)
Postprocessing	Data normalized at 10 mm from the applicator surface	

### TG-43 parameters for the INTRABEAM source with spherical applicators 7

where  $\dot{D}_i(10 \text{ mm}, \pi/2)$  is the dose rate measured at the reference point in water (DeWerd et al. 2015).

The origin of coordinates for calculations corresponds to the intersection of the source longitudinal axis with the external surface of the source needle (source tip). According to the manufacturer, this point coincides with the center of the spherical applicators.  $r$  distances were measured from the source tip and  $\theta = 0^\circ$  pointed towards the distal part of the probe as shown in figure 1(d).

*2.3.1. Air-kerma rate and dose-rate conversion coefficients.* NIST (or another PSDL) do not currently maintain a standard for the INTRABEAM system, and as such  $\dot{K}_{50\text{cm}}$  cannot be measured with traceability to a PSDL. For this study,  $\dot{K}_{50\text{cm}}$  was obtained from the air-kerma,  $K_{\text{air}}$ , calculated from the MC simulated fluence spectra in air at 50 cm from the source as

$$K_{\text{air}} = \sum_i \Phi_i E_i \left( \frac{\mu_{\text{tr}}}{\rho} \right)_{i,\text{air}}, \quad (3)$$

where  $\Phi_i$  is the photon fluence for energy bin  $i$ ,  $E_i$  is the photon bin energy, and  $(\mu_{\text{tr}}/\rho)_{i,\text{air}}$  is the mass energy transfer coefficient of air. Mass energy transfer coefficients can be obtained with the EGSnrc application  $g$  (Mainegra-Hing et al. 2020). The fluence spectra,  $\Phi_i$ , was obtained with MC using the spectrum scoring option *energy fluence in region* in `egs_brachy`. The simulations were run from the ring-shaped electron beam inside the source probe with  $3 \times 10^8$  starting histories for each applicator and the bare probe. For the geometry, the source with applicator was immersed in a 700 mm radius sphere of air with relative humidity of 40% as recommended by TG-43U1. Exploiting the azimuthal symmetry of the system, the scoring volume consisted of an annular air region of 1 mm radial thickness (inner radius 499.5 mm, outer radius 500.5 mm) and 10 mm axial thickness (in the  $z$  range -5.0 to 5.0 mm).

The MC simulations gave photon fluence per history in units of  $1/(\text{cm}^2 \text{ hist})$ , and  $K_{\text{air}}$  data were calculated with (3) in units of  $\text{MeV}/(\text{g hist})$ .  $\dot{K}_{50\text{cm}}$  values are then calculated as

$$\dot{K}_{50\text{cm}} = \left( \frac{K_{\text{air}}}{\text{hist}} \right) I, \quad (4)$$

where  $I$  is the beam current. Since the INTRABEAM is operated at a current of  $40 \mu\text{A} = (4/1.6 \times 10^{-14}) \text{ hist/s}$ ,  $\dot{K}_{50\text{cm}}$  values were calculated in units of  $\text{Gy/s}$  by applying a factor of  $4 \times 10^4$  to the  $K_{\text{air}}/\text{hist}$  results. Subsequently,  $\chi_i$  values were obtained for each applicator using the  $\dot{D}_i(10 \text{ mm}, \pi/2)$  values from the simulations in water.

### 2.4. Source calibration

The INTRABEAM system is calibrated by Zeiss using a PTW 23342 soft x-ray ionization chamber in water with a dedicated waterproof holder (Culberson et al. 2020, Shaikh et al. 2020). The PTW 23342 is a large-body parallel-plate ionization chamber with

### *TG-43 parameters for the INTRABEAM source with spherical applicators*

a collecting air volume of  $0.02 \text{ cm}^3$ . The chamber is calibrated in terms of exposure and the measurements are converted to absorbed dose rates to water by means of the so-called  $f$ -factor, which is obtained from ICRU Report 17 for 20 keV monoenergetic photons (ICRU 1970). As discussed by Watson et al. (2017, 2018, 2019), the  $f$ -factor does not account for spectral variations in energy for INTRABEAM photons at different depths in water. This dosimetry procedure is called the TARGIT dose-rate method, as it was used to determine dose-rate data for the TARGIT-A clinical trial for breast cancer (Vaidya et al. 2014).

The source manufacturer provides a dedicated phantom called INTRABEAM Water Phantom (Carl Zeiss Meditec AG 2011) that can be used in the clinic to verify the depth dose profiles from calibration. Measurements with this phantom are performed with a different ionization chamber, the PTW 34013, which is calibrated in terms of air-kerma. In order to compare the measurements in the clinic with the PTW 34013 chamber to the TARGIT-based calibration data, a depth-dependent correction factor must be applied. While this correction factor is an aggregate of several effects, its dominant contribution is the volume averaging of a detector, especially close to the source (Culberson et al. 2020). Since 2016, depth dose calibration data with the PTW 34013 chamber are measured by the manufacturer using the so-called V4.0 calibration method (Shaikh et al. 2020). V4.0 and TARGIT calibration data are provided with each INTRABEAM source in the form of dose-rate tables measured at different distances from the source tip in the range 3 to 45 mm in 0.5 mm steps. Depth-dependent applicator transfer functions are calculated as the ratio of doses measured with and without the applicator. Applicator transfer functions are also provided in a separate file.

#### *2.5. Validation of the MC model*

The MC model of the source was validated by comparing depth dose calculations in water for each spherical applicator against depth dose calibration data provided by Zeiss using the V4.0 calibration method. Data used to validate the MC model correspond to the calculations of the dose rates along the source longitudinal axis at distances measured from the source tip. Calibration dose rates of each applicator were obtained by multiplying the V4.0 dose rates of the bare probe by the corresponding transfer function. Depth dose curves were normalized at 10 mm from the applicator surface.

In contrast to the TG-43 formalism, Zeiss defines anisotropy as the relative percent difference of the dose at a certain point to the value at the same distance along  $\theta = 0^\circ$ , and not  $\theta = 90^\circ$  (Carl Zeiss Meditec AG 2011). The applicator anisotropy,  $A_{\text{iso}}$ , is defined by Zeiss as the difference of the source with applicator anisotropy,  $(X+A)_{\text{iso}}$ , and the bare probe anisotropy,  $X_{\text{iso}}$ :

$$A_{\text{iso}} = (X + A)_{\text{iso}} - X_{\text{iso}}. \quad (5)$$

The applicator calibration file provided by the manufacturer includes measured applicator anisotropies at 10 mm from the applicator surface. These values were calculated with our MC model and the results were compared to the calibration data.

TG-43 parameters for the INTRABEAM source with spherical applicators 9

**Table 2.** Uncertainty budget for the MC calculation of the dose rate at the reference point,  $\dot{D}_i(10 \text{ mm}, \pi/2)$ , for all spherical applicators. Since the Al filter is not present in the applicators with diameters 35 to 50 mm, the corresponding uncertainty cells were marked as ‘NA’.

Uncertainty component	Applicator diameter [mm]							
	15	20	25	30	35	40	45	50
<b>MC calculation</b>								
Statistical uncertainty [%]	0.03	0.03	0.03	0.03	0.03	0.03	0.03	0.04
Al filter geometry [%]	0.4	0.3	0.3	0.4	NA	NA	NA	NA
Standard uncertainty (k = 1) [%]	0.4	0.3	0.3	0.4	0.03	0.03	0.03	0.04
Expanded uncertainty (k = 2) [%]	<b>0.8</b>	<b>0.6</b>	<b>0.6</b>	<b>0.8</b>	<b>0.06</b>	<b>0.06</b>	<b>0.06</b>	<b>0.06</b>

### 3. Results and Discussion

#### 3.1. Uncertainty analyses

Uncertainties on  $\dot{D}_i(10 \text{ mm}, \pi/2)$  calculations were obtained following the recommendations of the International Organization for Standardization Guide to the Expression of Uncertainty in Measurement (ISO GUM) (BIPM, IEC, IFCC, ISO, IUPAC, IUPAP and OIML 1995) adapted for photon-emitting brachytherapy sources in the TG-138 report (DeWerd et al. 2011). Type A uncertainties of the simulations correspond to the statistical fluctuations per scoring volume reported in a ‘.3ddose’ file. The k = 1 statistical uncertainties in the  $\dot{D}_i(10 \text{ mm}, \pi/2)$  simulations were  $\sim 0.03\%$ , averaged for all applicators. As a type B uncertainty, the effect of the tolerance in the fabrication of the Al filter for the smallest applicators was evaluated, comparing the dose output of the thinner and thicker versions of it to that of the nominal dimensions. The axial position of the filter relative to the probe location was also varied according to the given construction tolerances. The estimated geometry uncertainties for  $\dot{D}_i(10 \text{ mm}, \pi/2)$  were up to 0.4%. This leads to combined standard uncertainties (k = 1) for the MC calculations of up to 0.4% for smaller applicators and 0.04% for larger applicators at the reference position. Uncertainties in the small applicators were therefore dominated by geometry tolerances of the Al filter. The uncertainty budget is presented in table 2. A confidence level of 95% in the calculations is obtained by providing expanded uncertainties to a coverage factor of two (k = 2).

The statistical uncertainties on the depth dose to water simulations along the source axis were below 0.9% for all applicators. The maximum uncertainty was reported for the furthest position from the surface of the 50 mm diameter applicator, and it is due to reduced fluence in the most distant voxel. The uncertainties along the source axis due to the Al filter tolerances were larger as getting close to the Al filter, thus the maximum was found at the surface of the 15 mm diameter applicator with a value of 2.0%. The total MC combined uncertainties along the source axis were below 2.0% and were dominated by the geometry contribution of the Al filter tolerances in the smallest applicators. The

**Table 3.** Uncertainty on the calibration dose rate data at 10 mm from the spherical applicators' surface, along the source probe axis, due to positioning tolerances.

Uncertainty component	Applicator diameter [mm]							
	15	20	25	30	35	40	45	50
<b>Calibration data</b>								
Position (plus radius) [mm]	0.5	0.5	0.4	0.6	0.7	0.7	0.6	0.7
Position (minus radius) [mm]	-0.4	-0.5	-0.5	-0.3	0.0	0.0	0.0	0.0
Positional uncertainty [%]	<b>6.3</b>	<b>6.1</b>	<b>4.2</b>	<b>4.6</b>	<b>4.2</b>	<b>3.9</b>	<b>2.8</b>	<b>3.1</b>

total uncertainties on the normalized MC depth dose curves were calculated through uncertainty propagation and were all below 2.4% with a maximum at the surface of the 15 mm diameter applicator.

Calibration data are provided by the manufacturer with applicator positional tolerances in the radial direction (plus and minus) as shown in table 3 for all applicators. The influence of the positioning tolerances on the dosimetric uncertainty was determined as the difference in dose rate at each depth in water when applying a positional offset to the fitted depth dose curve. The dose rate positional uncertainties are dependent on the slope of the dose fall-off, which will depend on the distance from the source tip and the beam hardening through the applicator materials. For instance, the largest dose rate positional uncertainty is 12.5% and it is observed at the surface of the 15 mm diameter applicator, which is the closest point to the source tip. The corresponding uncertainties at 10 mm from the applicators' surface, along  $\theta = 0^\circ$ , varied from 2.8% to 6.3% for all applicators.

The geometry uncertainties on the MC calculated dose rates, due to the tolerance on the thickness of the Al filter, are dependent on the polar angular position around the applicator. This behaviour is presented in figure 2 for the smallest applicators as calculated at 10 mm from the applicator surface in the polar angular range  $\theta = 0^\circ$  to  $160^\circ$ . It is to be noticed from the figure, however, that the geometry uncertainties at the reference point were close to their minimum, compared to the larger values at the positions proximal to the source axis, with a maximum exhibited towards the forwarded beam direction, reaching a value of  $\sim 1.5\%$  at  $\theta = 0^\circ$  for the 20 mm diameter applicator.

### 3.2. Validation of the MC model

The in-water depth dose curves calculated along the source axis with MC for the eight applicators are shown in figure 3 together with the calibration measurements provided in the Zeiss calibration data tables. For the latter, the V4.0 method was used, whereby the depth-dependent transfer function parameters specific to each applicator were multiplied by the dose at the same depth for the bare probe. All curves are normalized to unity at a depth of 10 mm from the applicator surface. All distances are measured from the source tip and only data outside the applicators' volume is presented in figure 3. The

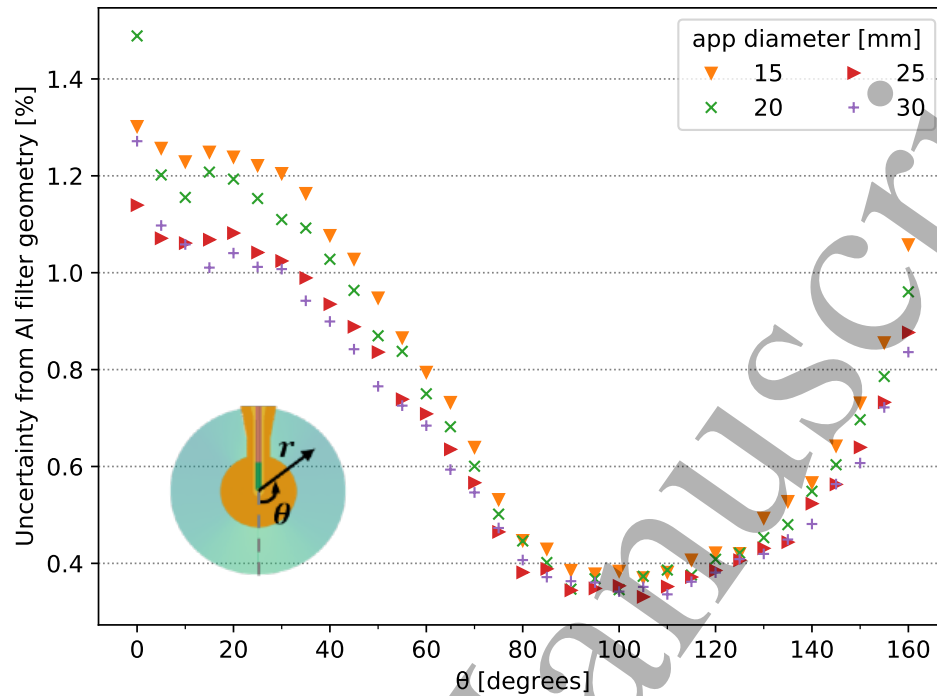


**Figure 2.** Dose calculation uncertainties due to geometry variations of the Al filter construction within tolerance values. The curves shown were calculated at 10 mm from the applicator surface for the smallest applicators of diameters 15 to 30 mm.

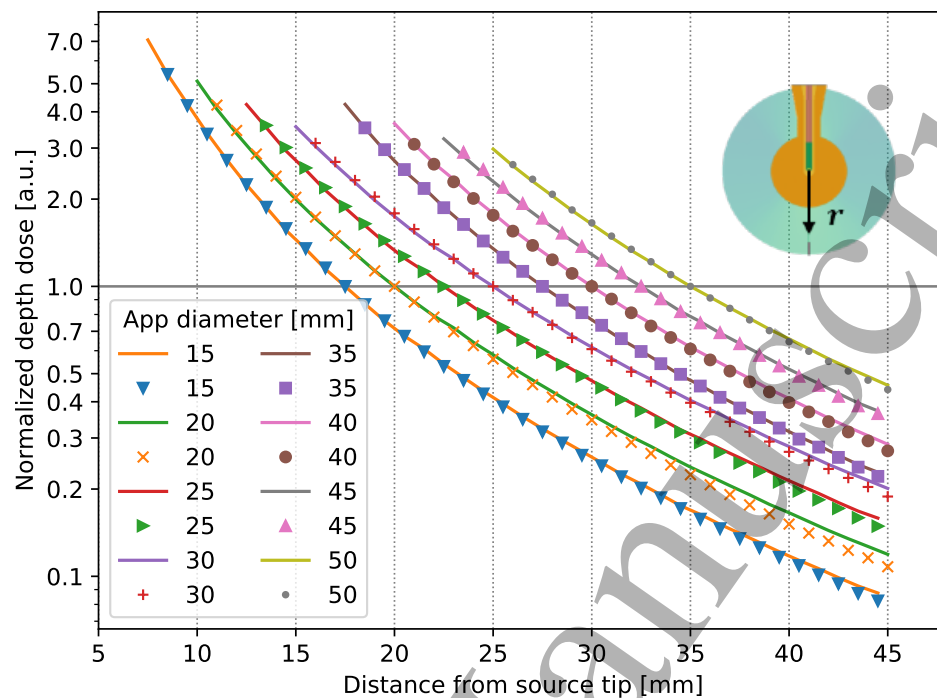
plots are shown on a log-linear scale to better appreciate the local relative differences at deeper positions in water.

Figure 4 presents the local relative differences of the MC simulated dose profiles and the calibration data for all applicators along the source central axis. The error bars in the figure represent the combined standard uncertainties of the difference, with coverage factor 1 ( $k = 1$ ). In general, these combined uncertainties were strongly dominated by calibration positional uncertainties, especially close to the source, due to the steep gradients in dose distribution. At distances of up to 30 mm from the source tip, the observed local relative differences were within the total uncertainties. At depths beyond 30 mm, MC calculations exhibit local relative differences from calibration data of up to 8% for the 20 mm diameter applicator and were larger for the smallest applicators. The larger discrepancies exhibited in the smallest applicators can be correlated to the uncertainties of their Al filter construction shown in table 2. However, the differences were still within  $k = 2$  standard uncertainties, validating the MC model.

The calculated applicator anisotropy, as described by Zeiss according to (1), is shown in figure 5 as obtained at 10 mm from all the applicators' surface, in the polar angle range  $\theta = 0^\circ$  to  $130^\circ$ . The error bars included in the plots correspond to the combined standard uncertainties accounting for the tolerances in the Al filter manufacturing for the smallest applicators and statistical fluctuations in the simulations.

The calibration data include measured polar anisotropies for each spherical

TG-43 parameters for the INTRABEAM source with spherical applicators 12



**Figure 3.** Depth-dose curves along the source longitudinal axis for the INTRABEAM system with spherical applicators ranging in diameter from 15 mm to 50 mm in steps of 5 mm. The curves are normalized at 10 mm from the applicator surface. The distances shown are measured from the source tip. The MC calculated data (marks only) are compared to the data provided by the manufacturer (Carl Zeiss) in the calibration file (solid lines).

applicator which ranged between -8.1% and 5.9%. All the MC calculated anisotropies in this study were found within the provided exemplary calibration data. This result is consistent with that provided by Shamsabadi et al. (2020), who reported anisotropies in the same range at 10 mm distance from the applicators' surface.

### 3.3. Photon fluence spectra, air-kerma rates and dose-rate conversion coefficients.

The MC simulated photon fluence spectra scored in air at 50 cm from the source tip are presented in figure 6. Figure 6(a) shows the spectrum of the bare probe and the spectra of the source with spherical applicators of various diameters are presented in figure 6(b). The spectral change caused by the presence of the applicators, relative to the bare probe spectrum, is noticeable in figure 6 as a decrease in the intensity of the fluorescence peaks and a large relative contribution of bremsstrahlung x-rays. For the low-energy range of the spectrum, the Coulombic interactions of the incoming electrons with the orbital electrons of the K and L shells of the gold target and nickel wall atoms play a significant role in the x-ray production inside the INTRABEAM needle. Atomic relaxation leads to fluorescence photons with a photon spectrum dominated by the fluorescence L-lines of gold (in the range 9 to 14 keV) and K-lines of nickel (7.5

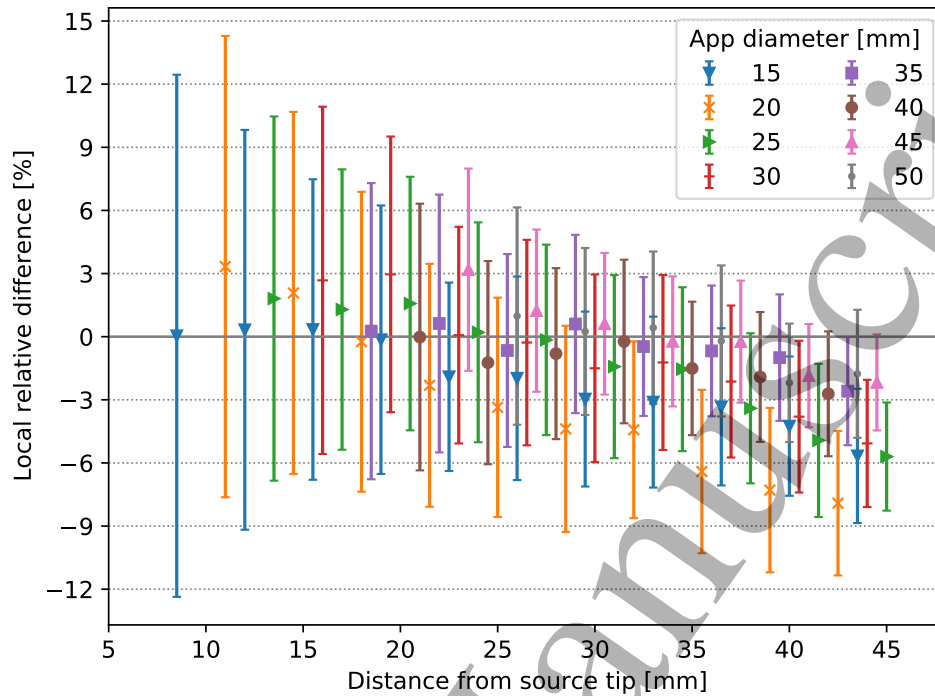


**Figure 4.** Deviations from MC simulations to calibration data provided by the source manufacturer (Carl Zeiss), expressed as local relative differences, for the INTRABEAM source with each of the eight spherical applicators.

and 8.3 keV) (Watson et al. 2017, Yanch & Harte 1996, Nwankwo et al. 2013, Moradi et al. 2017). The presence of the Al filter in the smallest applicators hardens the photon beam, resulting in a marked effect on the spectral distribution exhibited as a greater attenuation of characteristic x-ray peaks. As seen in figure 6(b), the bremsstrahlung peak is displaced towards higher energies for applicators with Al filter and in proportion with the diameter of the polyetherimide sphere. The fluence averaged energy,  $\bar{E}_\Phi$ , the total photon fluence,  $\Phi$ , and the fluence averaged transfer coefficients,  $(\mu_{tr}/\rho)_{air,\Phi}$ , were calculated at the scoring voxel for the bare probe and for the source with applicators of increasing diameter from 15 to 50 mm, and are reported in table 4.

The air-kerma data for each applicator were obtained from the spectra in air using (3), and the corresponding air-kerma rates calculated with (4) for a current of 40  $\mu\text{A}$  are presented in table 4. As an approximate calculation test using the fluence averaged energies and transfer coefficients from table 4 would give average  $K_{air}$  values of  $3.203 \times 10^{-9}$  and  $4.021 \times 10^{-10}$  MeV/(g hist) for the bare probe and the 40 mm diameter applicator, for example, which from (4) and a current of 40  $\mu\text{A}$  would give  $\dot{K}_{50\text{cm}}$  values of  $12.81 \times 10^{-2}$  and  $1.413 \times 10^{-2}$  mGy/s, which coincide with the calculated values reported in table 4.

$\dot{D}(10\text{ mm}, \pi/2)$  values were obtained from the MC calculations performed for the relative TG-43 parameters in water and are also reported in table 4, followed by the corresponding dose-rate conversion coefficients,  $\chi$ , calculated for the bare probe and the

## TG-43 parameters for the INTRABEAM source with spherical applicators 14

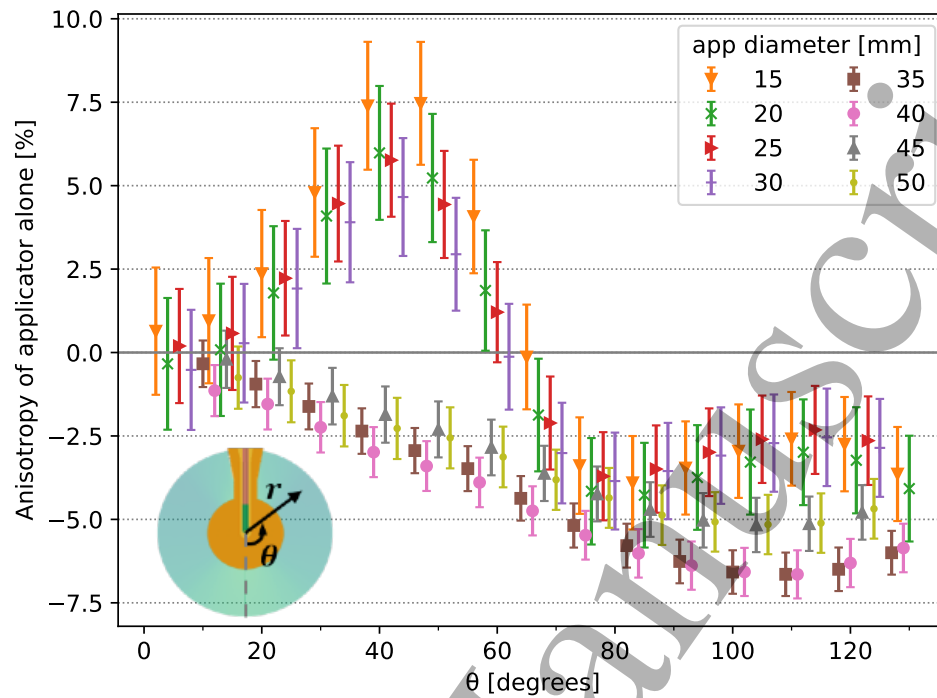


**Figure 5.** MC calculated anisotropy of the spherical applicators alone (after subtracting the bare probe anisotropy), at 10 mm from the applicators' surface, along the angular range  $\theta = 0^\circ$  to  $130^\circ$ . The applicator anisotropy was calculated according to the manufacturer specifications (Carl Zeiss) relative to  $\theta = 0^\circ$  and subtracting the bare probe anisotropy.

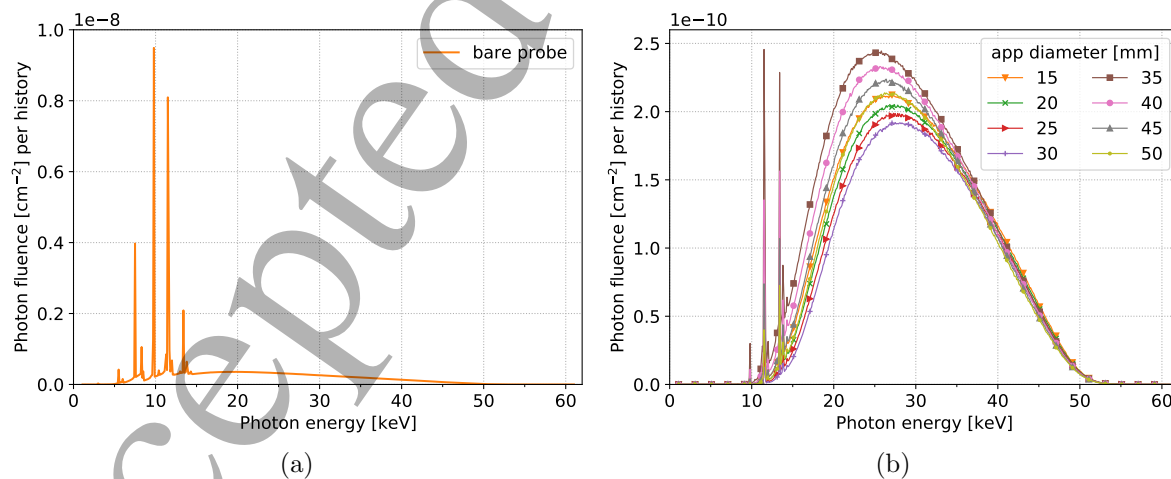


**Figure 6.** Photon fluence spectra scored in air at 50 cm from the source axis in an annular volume for (a) the INTRABEAM bare probe and (b) the INTRABEAM source with spherical applicators.

source with applicators.

TG-43 parameters for the INTRABEAM source with spherical applicators 15

**Table 4.** Total photon fluence,  $\Phi$ , fluence averaged energy,  $\bar{E}_\Phi$ , fluence averaged transfer coefficient,  $(\mu_{tr}/\rho)_{air,\Phi}$ , and air-kerma rate,  $\dot{K}_{50cm}$ , calculated from the photon fluence spectra at 50 cm from the source tip (at  $\theta = 90^\circ$ ), absorbed-dose rate to water at the reference point of 10 mm from the applicator surface,  $\dot{D}(10\text{ mm}, \pi/2)$ , and dose-rate conversion coefficient,  $\chi$ , for the INTRABEAM bare probe and all spherical applicators. The data shown were calculated for the system operated at a current of 40  $\mu\text{A}$ .

Parameter	Bare probe	Applicator diameter [mm]							
		15	20	25	30	35	40	45	50
$\Phi$ [ $\times 10^{-8}$ cm $^{-2}$ hist $^{-1}$ ]	12.98	4.81	4.57	4.35	4.15	5.54	5.17	4.86	4.57
$\bar{E}_\Phi$ [keV]	20.4	29.8	30.1	30.3	30.5	28.5	28.9	29.3	29.6
$(\mu_{tr}/\rho)_{air,\Phi}$ [cm $^2$ /g]	1.211	0.212	0.202	0.194	0.188	0.255	0.236	0.222	0.211
$\dot{K}_{50cm}$ [ $\times 10^{-2}$ mGy/s]	12.81	1.216	1.111	1.026	0.952	1.608	1.413	1.263	1.142
$\dot{D}(10\text{ mm}, \pi/2)$ [mGy/s]	55.60	8.310	6.093	4.613	3.582	4.036	3.187	2.561	2.085
$\chi$	434.0	683.5	548.3	449.9	376.5	251.0	225.6	202.8	182.6

### 3.4. Radial dose function

The calculated radial dose functions for the INTRABEAM source with the spherical applicators are shown in figure 7. The function has been calculated from the applicator surface to 50 mm from the source tip. Figure 7 is presented in terms of the distance from applicator surface. As recommended in the TG-43 formalism, the radial dose functions were obtained along  $\theta = 90^\circ$  taking as reference position the point located at 10 mm from the applicator surface. A point-source approximation was used, thus the inverse square law behaviour accounted for in the geometry function of (1) was removed in the calculated radial dose function. The function data for all applicators are presented also in table A1 for distances from the source tip in the range 2 to 50 mm. For completeness, the radial dose function of the INTRABEAM bare probe previously reported by Ayala Alvarez et al. (2020) is also presented in this table. The  $k = 1$  type A uncertainties of the MC simulations with applicators, not shown in the table, varied from 0.03% to 0.05%, with the maximum obtained at 50 mm for the case of the 50 mm diameter applicator.

As can be observed in figure 7, the radial dose function behaviour is split in two groups of applicator diameters. The applicators with larger diameters of 35 to 50 mm exhibit a steeper radial dose function than that of the smaller applicators. The flattened behaviour observed in the smallest applicators is due to the beam hardening occurring at the Al filter (Al filter is not present in larger applicators). Spectral variations of the incoming beams, as they pass through different media, are more prominent at smaller distances from the source as inferred from the curves separation near the applicators' surface and the smoother and converging behaviour of the curves as moving away from the source tip. Because the Al filter pre-hardens the beam, as seen in the average photon energy for each applicator (table 4), there is less beam hardening occurring through the

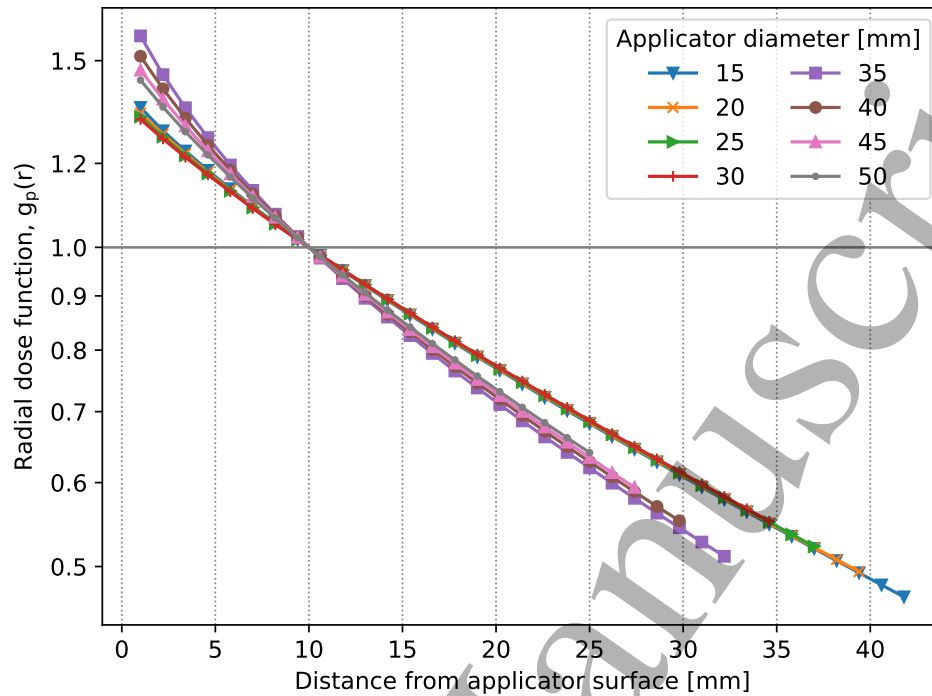


**Figure 7.** Radial dose functions for the INTRABEAM system with the available spherical applicators. The subscript “p” indicates that a point-source approximation was used in the calculations. The enhanced penetration of the smallest applicators is attributed to the beam pre-hardening throughout the added aluminium filter.

water, hence the less steep radial dose function of the smallest applicators.

### 3.5. 2D anisotropy function

The TG-43 2D anisotropy functions were calculated with the validated MC model of the source with all the spherical applicators. Based on the source construction specifications, azimuthal symmetry was assumed. As example, the polar anisotropy of the 40 mm diameter applicator is presented in figure 8 at different distances from the applicator surface as a function of polar angle ( $\theta$ ). Since the 2D anisotropy is calculated only outside the applicator, the data is presented between  $\theta = 0^\circ$  and up to  $\theta \approx 160^\circ$ . Some dosimetry aspects can be inferred from figure 8. For instance, a larger anisotropy is observed near the source axis, towards  $\theta = 0^\circ$  and  $\theta = 180^\circ$ , indicating a strong contribution from primary and back-scattered components of the beam compared to the transverse dose delivered with the system. The forward directed anisotropy is larger, reaching values of up to 27%, which can be related to the selection of the system’s origin at the outer surface of the source tip instead of the effective source position. These effects were also exhibited in the published bare probe anisotropy data (Ayala Alvarez et al. 2020). Calculated 2D anisotropy data for all the applicators are presented in tables A2 to A4 for polar angles  $0^\circ$  to  $170^\circ$  in steps of  $5^\circ$  and different radial distances from the source

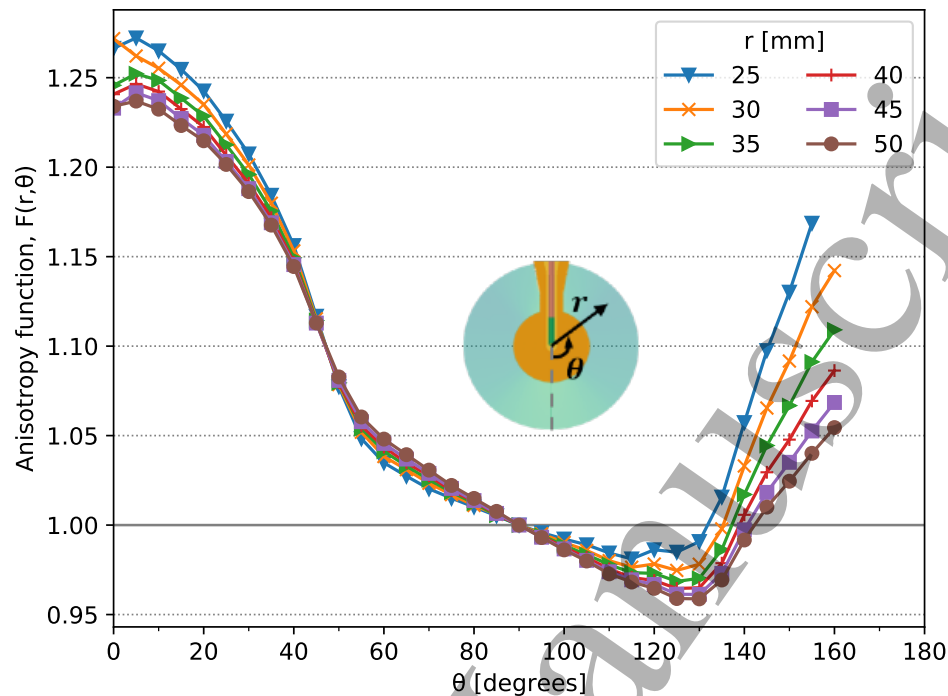


**Figure 8.** 2D anisotropy function of the INTRABEAM source with the 40 mm diameter applicator calculated at several distances from the source tip in the polar angle range  $\theta = 0^\circ$  to  $160^\circ$ .

tip. The radial and angular binning used to generate the provided 2D anisotropy tables permit linear-linear interpolation resulting in differences no larger than  $\pm 2\%$  from the MC calculations, as recommended in the TG-43U1 protocol.

The polar anisotropy at 10 mm from the applicator surface is presented in figure 9 for all the applicators as a function of polar angle. For the smallest applicators, the effect of the Al filter is exhibited as a decrease in anisotropy close to the source axis, towards  $\theta = 0^\circ$  and  $\theta = 180^\circ$ , where the back-scattered beam is shielded along a larger relative path through aluminium. When comparing the 2D anisotropy at 10 mm from the applicators' surface to that previously reported for the bare probe by Ayala Alvarez et al. (2020), a less homogeneous dose distribution is exhibited at  $\theta$  angles  $0^\circ$  to  $90^\circ$  with the presence of the applicators, whereas the reverse effect was observed at angles  $90^\circ$  to  $180^\circ$ . This phenomenon can be attributed to the larger added attenuation material of the applicators towards the transverse reference line compared to that added in the forward direction of the beam from the source effective position. The increased relative x-ray filtration towards the reference line makes the 2D anisotropy values larger at small angles. The added forward anisotropy with the presence of the applicators was also reported by Shamsabadi et al. (2020) and Eaton et al. (2013).

TG-43 parameters for the INTRABEAM source with spherical applicators 18

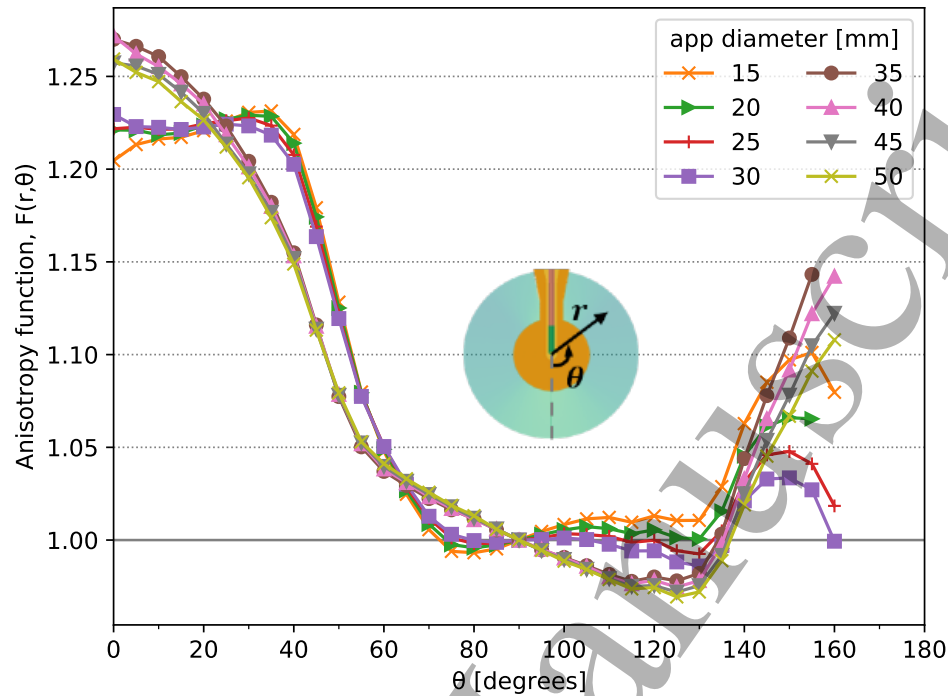


**Figure 9.** 2D anisotropy function curves calculated at 10 mm from the surface of the INTRABEAM spherical applicators in the polar angle range  $\theta = 0^\circ$  to  $160^\circ$ .

#### 4. Conclusion

The dosimetric parameters recommended by the TG-43 formalism and adapted for eBT sources were calculated with MC for the INTRABEAM source with the eight spherical applicators. Specifically, the air-kerma rate at 50 cm, the dose-rate conversion coefficients, the radial dose function and the 2D-anisotropy function for the INTRABEAM system were obtained and tabulated. The MC model was validated with calibration data provided by the manufacturer, with local relative differences found within the estimated uncertainties. The present work strengthens the conjoint effort towards the dosimetry standardization of eBT by showing the feasibility of its application to the INTRABEAM system with the spherical applicators of common clinical use in IORT. A dose to water method was employed in which the dose-rate to water at a reference point is obtained from calibration air-kerma rates in measurement conditions using a MC calculated dose-rate conversion coefficient. It is to be noted, however, that the calculated dose-rate conversion coefficients can differ from the calibration ones once a consensus on the measurement of air-kerma rate at a primary standards dosimetry laboratory has been reached. This is akin to the multiplicity of dose-rate constants available for a given brachytherapy source, as stated in the TG-43U1 (Rivard et al. 2004), depending on the calibration standard to which the reference dose rate was normalized.

Although the results were obtained herein for a dedicated source and applicator,

1  
2 *TG-43 parameters for the INTRABEAM source with spherical applicators* 19  
3

4 the methodology can be extended to other applicators and eBT sources. The data  
5 reported in this manuscript can be used to feed a TPS to obtain dose distributions in  
6 IORT applications where the surrounding tissues are considered water-equivalent for  
7 low-energy photons. Further research is needed to assess the implementation of the  
8 data obtained with the TG-43 formalism and correct for tissue heterogeneities in more  
9 general patient-specific calculations.  
10  
11  
12

### 13 14 **Acknowledgments** 15

16 The authors wish to thank Mathias Benker of Carl Zeiss for details on the INTRABEAM  
17 spherical applicators. D.S.A.A. acknowledges the financial support from the Fonds de  
18 recherche du Québec – Santé (FRQS, grant number: 292924). This work was presented  
19 at the COMP Annual Scientific Meeting 2021, virtual meeting, June 22–25, 2021.  
20  
21  
22

### 23 **Appendix** 24

25 The following tables in this section summarize the relative TG-43 parameters,  $g_p(r)$   
26 and  $F(r, \theta)$ , calculated with MC for the INTRABEAM source with the eight available  
27 spherical applicators.  
28  
29  
30  
31  
32  
33  
34  
35  
36  
37  
38  
39  
40  
41  
42  
43  
44  
45  
46  
47  
48  
49  
50  
51  
52  
53  
54  
55  
56  
57  
58  
59  
60

*TG-43 parameters for the INTRABEAM source with spherical applicators* 20

**Table A1.** MC calculated radial dose function data,  $g_p(r)$ , for the INTRABEAM bare probe and with spherical applicators. The TG-43 point-source model has been used. Points located inside the applicator, for which  $g_p(r)$  is not determined, are indicated by 'NA'.

$r$ [mm]	bare probe	Applicator diameter [mm]							
		15	20	25	30	35	40	45	50
2	4.782	NA	NA	NA	NA	NA	NA	NA	NA
4	2.510	NA	NA	NA	NA	NA	NA	NA	NA
6	1.645	NA	NA	NA	NA	NA	NA	NA	NA
8	1.232	1.381	NA						
10	1.000	1.274	1.362	NA	NA	NA	NA	NA	NA
12	0.854	1.186	1.288	1.249	NA	NA	NA	NA	NA
14	0.753	1.111	1.201	1.303	NA	NA	NA	NA	NA
16	0.678	1.045	1.126	1.217	1.320	NA	NA	NA	NA
18	0.619	0.986	1.059	1.141	1.232	1.639	0.105	NA	NA
20	0.571	0.933	1.000	1.074	1.156	1.428	1.593	NA	NA
22	0.530	0.884	0.946	1.014	1.088	1.276	1.427	1.444	NA
24	0.495	0.839	0.897	0.960	1.028	1.157	1.285	1.430	NA
26	0.464	0.798	0.852	0.910	0.973	1.061	1.172	1.296	1.438
28	0.436	0.760	0.810	0.864	0.923	0.981	1.079	1.187	1.308
30	0.411	0.724	0.771	0.821	0.876	0.911	1.000	1.096	1.203
32	0.388	0.690	0.734	0.782	0.833	0.851	0.932	1.018	1.113
34	0.367	0.659	0.700	0.745	0.793	0.797	0.870	0.949	1.036
36	0.348	0.629	0.668	0.710	0.755	0.748	0.816	0.888	0.967
38	0.330	0.601	0.638	0.677	0.720	0.704	0.767	0.834	0.906
40	0.313	0.574	0.609	0.646	0.687	0.665	0.723	0.785	0.851
42	0.298	0.549	0.582	0.617	0.655	0.628	0.682	0.740	0.802
44	0.283	0.526	0.557	0.590	0.626	0.595	0.645	0.698	0.756
46	0.270	0.503	0.533	0.564	0.598	0.563	0.611	0.660	0.715
48	0.257	0.482	0.510	0.540	0.572	0.534	0.579	0.625	0.676
50	0.245	0.461	0.488	0.517	0.547	0.507	0.549	0.592	0.640

*TG-43 parameters for the INTRABEAM source with spherical applicators* 21

**Table A2.** MC calculated 2D anisotropy function data,  $F(r, \theta)$ , for the INTRABEAM source with the 15 and 20 mm diameter spherical applicators. Points located inside the applicators, for which  $F(r, \theta)$  is not determined, are indicated by 'NA'.

$\theta$ [°]	Radial distance from the source tip, $r$ [mm]													
	Applicator 15 mm							Applicator 20 mm						
	8	10	15	20	30	40	50	12	15	20	30	40	50	
0	1.118	1.155	1.197	1.207	1.228	1.239	1.238	1.177	1.199	1.221	1.235	1.211	1.193	
5	1.119	1.158	1.204	1.221	1.228	1.230	1.227	1.183	1.204	1.221	1.228	1.228	1.229	
10	1.127	1.163	1.207	1.221	1.229	1.227	1.227	1.186	1.204	1.219	1.226	1.227	1.226	
15	1.134	1.167	1.209	1.221	1.227	1.225	1.225	1.188	1.206	1.219	1.225	1.224	1.221	
20	1.145	1.177	1.214	1.224	1.225	1.221	1.218	1.199	1.214	1.224	1.224	1.221	1.216	
25	1.165	1.194	1.221	1.227	1.224	1.218	1.213	1.211	1.222	1.227	1.222	1.217	1.211	
30	1.191	1.212	1.230	1.229	1.220	1.211	1.205	1.226	1.230	1.229	1.220	1.211	1.203	
35	1.217	1.230	1.234	1.227	1.213	1.201	1.194	1.238	1.235	1.228	1.212	1.200	1.192	
40	1.231	1.233	1.224	1.213	1.195	1.184	1.176	1.234	1.226	1.214	1.195	1.184	1.175	
45	1.211	1.202	1.185	1.173	1.158	1.150	1.145	1.200	1.187	1.174	1.158	1.149	1.143	
50	1.165	1.150	1.133	1.124	1.116	1.112	1.110	1.146	1.135	1.125	1.116	1.111	1.109	
55	1.108	1.093	1.082	1.078	1.078	1.078	1.081	1.091	1.083	1.079	1.077	1.078	1.079	
60	1.058	1.049	1.047	1.049	1.054	1.057	1.061	1.049	1.048	1.049	1.053	1.057	1.059	
65	1.018	1.016	1.021	1.027	1.035	1.041	1.045	1.019	1.021	1.027	1.034	1.040	1.043	
70	0.988	0.990	1.001	1.009	1.020	1.026	1.031	0.995	1.001	1.009	1.019	1.025	1.029	
75	0.970	0.974	0.989	0.998	1.009	1.016	1.020	0.980	0.989	0.998	1.008	1.015	1.018	
80	0.969	0.975	0.989	0.996	1.004	1.009	1.012	0.982	0.988	0.996	1.004	1.008	1.011	
85	0.982	0.986	0.993	0.997	1.001	1.004	1.006	0.990	0.993	0.997	1.001	1.004	1.004	
90	1.000	1.000	1.000	1.000	1.000	1.000	1.000	1.000	1.000	1.000	1.000	1.000	1.000	
95	1.020	1.014	1.007	1.002	0.999	0.997	0.996	1.012	1.007	1.003	0.999	0.997	0.995	
100	1.041	1.028	1.012	1.005	0.997	0.993	0.991	1.022	1.013	1.005	0.997	0.993	0.990	
105	1.060	1.041	1.018	1.006	0.995	0.989	0.986	1.031	1.018	1.007	0.995	0.989	0.985	
110	1.074	1.050	1.021	1.005	0.992	0.984	0.979	1.038	1.021	1.006	0.991	0.985	0.979	
115	1.085	1.055	1.019	1.002	0.987	0.979	0.974	1.040	1.020	1.003	0.987	0.979	0.973	
120	1.092	1.061	1.024	1.005	0.985	0.975	0.969	1.045	1.026	1.005	0.985	0.975	0.969	
125	1.110	1.072	1.024	1.000	0.977	0.966	0.961	1.052	1.026	1.001	0.978	0.967	0.960	
130	1.127	1.081	1.026	0.999	0.975	0.963	0.957	1.057	1.028	1.001	0.975	0.963	0.956	
135	1.168	1.114	1.047	1.015	0.984	0.969	0.960	1.084	1.048	1.016	0.984	0.969	0.960	
140	1.232	1.168	1.086	1.045	1.005	0.985	0.973	1.127	1.086	1.045	1.005	0.985	0.972	
145	1.274	1.205	1.112	1.065	1.018	0.994	0.980	1.155	1.108	1.061	1.015	0.993	0.978	
150	NA	1.232	1.127	1.075	1.022	0.996	0.981	1.162	1.114	1.066	1.017	0.994	0.978	
155	NA	NA	1.134	1.075	1.019	0.993	0.978	1.168	1.118	1.065	1.013	0.989	0.975	
160	NA	NA	NA	1.053	1.000	0.977	0.964	NA	1.102	1.047	0.997	0.975	0.962	
165	NA	NA	NA	1.007	0.961	0.947	0.941	NA	NA	1.003	0.959	0.947	0.940	
170	NA	NA	NA	NA	0.898	NA	NA	NA	NA	NA	0.897	NA	NA	





## References

- Abudra'A, A., Chauvenet, B., Gouriou, J., Plagnard, J., Itti, R. & Aubineau-Lanière, I. (2020). Dosimetry formalism and calibration procedure for electronic brachytherapy sources in terms of absorbed dose to water, *Physics in Medicine & Biology* **65**(14): 145006.
- Ayala Alvarez, D. S., Watson, P. G., Popovic, M., Heng, V. J., Evans, M. D. & Seuntjens, J. (2020). Monte Carlo calculation of the relative TG-43 dosimetry parameters for the INTRABEAM electronic brachytherapy source, *Physics in Medicine & Biology* **65**(24): 245041.
- Beaulieu, L., Carlsson Tedgren, Å., Carrier, J.-F., Davis, S. D., Mourtada, F., Rivard, M. J., Thomson, R. M., Verhaegen, F., Wareing, T. A. & Williamson, J. F. (2012). Report of the Task Group 186 on model-based dose calculation methods in brachytherapy beyond the TG-43 formalism: current status and recommendations for clinical implementation, *Medical physics* **39**(10): 6208–6236.
- Berger, M. J., Hubbell, J. H., Seltzer, S. M., Chang, J., Coursey, J. S., Sukumar, R., Zucker, D. S. & Olsen (2010). XCOM: Photon Cross Sections Database (version 1.5). [Online] Available: <http://physics.nist.gov/xcom> (accessed September 2020), *National Institute of Standards and Technology, Gaithersburg, MD* .  
**URL:** <http://physics.nist.gov/xcom>
- BIPM, IEC, IFCC, ISO, IUPAC, IUPAP and OIML (1995). Guide to the Expression of Uncertainty in Measurement, *Geneva, Switzerland: International Organisation for Standardisation* .
- Bote, D. & Salvat, F. (2008). Calculations of inner-shell ionization by electron impact with the distorted-wave and plane-wave Born approximations, *Physical Review A* **77**(4): 042701.
- Carl Zeiss Meditec AG (2011). *INTRABEAM dosimetry, Brochure EN\_30\_010\_155II*.
- Carl Zeiss Meditec AG (2017). *INTRABEAM System from ZEISS – Technical Specifications, EN\_30\_010\_0158IV*.
- Chamberland, M. J. P., Taylor, R. E. P., Rogers, D. W. O. & Thomson, R. M. (2016). egs\_brachy: a versatile and fast Monte Carlo code for brachytherapy, *Physics in Medicine & Biology* **61**(23): 8214–8231.
- Clausen, S., Schneider, F., Jahnke, L., Fleckenstein, J., Hesser, J., Glatting, G. & Wenz, F. (2012). A Monte Carlo based source model for dose calculation of endovaginal TARGIT brachytherapy with INTRABEAM and a cylindrical applicator, *Zeitschrift für Medizinische Physik* **22**(3): 197–204.
- Culberson, W. S., Davis, S. D., Gwe-Ya Kim, G., Lowenstein, J. R., Ouhib, Z., Popovic, M., Waldron, T. J., Safigholi, H., Simiele, S. J. & Rivard, M. J. (2020). Dose-rate considerations for the INTRABEAM electronic brachytherapy system: Report from the American association of physicists in medicine task group no. 292, *Medical physics* **47**(8): e913–e919.
- DeWerd, L. A., Culberson, W. S., Micka, J. A. & Simiele, S. J. (2015). A modified dose calculation formalism for electronic brachytherapy sources, *Brachytherapy* **14**(3): 405–408.
- DeWerd, L. A., Ibbott, G. S., Meigooni, A. S., Mitch, M. G., Rivard, M. J., Stump, K. E., Thomadsen, B. R. & Venselaar, J. L. (2011). A dosimetric uncertainty analysis for photon-emitting brachytherapy sources: Report of AAPM Task Group No. 138 and GEC-ESTRO, *Medical physics* **38**(2): 782–801.
- Dinsmore, M., Harte, K. J., Sliski, A. P., Smith, D. O., Nomikos, P. M., Dalterio, M. J., Boom, A. J., Leonard, W. F., Oettinger, P. E. & Yanch, J. C. (1996). A new miniature x-ray source for interstitial radiosurgery: Device description, *Medical Physics* **23**(1): 45–52.
- Eaton, D. (2012). Quality assurance and independent dosimetry for an intraoperative x-ray device, *Medical physics* **39**(11): 6908–6920.
- Eaton, D., Earner, B., Faulkner, P. & Dancer, N. (2013). A national dosimetry audit of intraoperative radiotherapy, *The British journal of radiology* **86**(1032): 20130447.
- Giordano, F. A., Brehmer, S., Abo-Madyan, Y., Welzel, G., Sperk, E., Keller, A., Schneider, F., Clausen, S., Herskind, C., Schmiedek, P. & Wenz, F. (2014). INTRAGO: intraoperative

*TG-43 parameters for the INTRABEAM source with spherical applicators* 25

- radiotherapy in glioblastoma multiforme – a Phase I/II dose escalation study, *BMC Cancer* **14**(1): 992.  
**URL:** <https://doi.org/10.1186/1471-2407-14-992>
- Giordano, F. A., Brehmer, S., Mürle, B., Welzel, G., Sperk, E., Keller, A., Abo-Madyan, Y., Scherzinger, E., Clausen, S. & Schneider, F. e. a. (2018). Intraoperative Radiotherapy in Newly Diagnosed Glioblastoma (INTRAGO): An Open-Label, Dose-Escalation Phase I/II Trial, *Neurosurgery* **84**(1): 41–49.
- Hiatt, J. R., Davis, S. D. & Rivard, M. J. (2015). A revised dosimetric characterization of the model S700 electronic brachytherapy source containing an anode-centering plastic insert and other components not included in the 2006 model, *Medical Physics* **42**(6Part1): 2764–2776.
- Hiatt, J. R., Rivard, M. J. & Hughes, H. G. (2016). Simulation evaluation of NIST air-kerma rate calibration standard for electronic brachytherapy, *Medical physics* **43**(3): 1119–1129.
- ICRU (1970). *Radiation Dosimetry: X Rays Generated at Potentials of 5 to 150 KV.*, Vol. 17, International Commission on Radiation Units and Measurements.
- Kawrakow, I., Mainegra-Hing, E., Tessier, F. & Walters, B. R. B. (2009). The EGSnrc C++ class library, NRC Report PIRS-898 (rev A), *Technical report*, National Research Council Canada, Ottawa, Canada.
- Kawrakow, I. & Rogers, D. W. O. (2019). The EGSnrc code system: Monte Carlo simulation of electron and photon transport, *Technical Report PIRS-701*, National Research Council Canada, Ottawa, Canada.  
**URL:** <http://nrc-cnrc.github.io/EGSnrc/doc/pirs701-egsnrc.pdf>
- Mainegra-Hing, E., Rogers, D., Townson, R., Walters, B., Tessier, F. & Kawrakow, I. (2020). The EGSnrc g application, *Technical Report PIRS-3100*, National Research Council Canada, Ottawa, Canada.  
**URL:** <https://nrc-cnrc.github.io/EGSnrc/doc/pirs3100/>
- Moradi, F., Ung, N. M., Khandaker, M. U., Mahdiraji, G. A., Saad, M., Abdul Malik, R., Bustam, A. Z., Zaili, Z. & Bradley, D. A. (2017). Monte Carlo skin dose simulation in intraoperative radiotherapy of breast cancer using spherical applicators, *Physics in Medicine & Biology* **62**(16): 6550–6566.
- Nath, R., Anderson, L. L., Luxton, G., Weaver, K. A., Williamson, J. F. & Meigooni, A. S. (1995). Dosimetry of interstitial brachytherapy sources: Recommendations of the AAPM Radiation Therapy Committee Task Group No. 43, *Medical Physics* **22**(2): 209–234.
- Nath, R., Rivard, M. J., DeWerd, L. A., Dezarn, W. A., Heaton, H. T., Ibbott, G. S., Meigooni, A. S., Ouhib, Z., Rusch, T. W., Siebert, F.-A. et al. (2016). Guidelines by the AAPM and GEC-ESTRO on the use of innovative brachytherapy devices and applications: Report of Task Group 167, *Medical physics* **43**(6Part1): 3178–3205.
- Nwankwo, O., Clausen, S., Schneider, F. & Wenz, F. (2013). A virtual source model of a kilo-voltage radiotherapy device, *Physics in Medicine & Biology* **58**(7): 2363–2375.
- Rivard, M. J., Coursey, B. M., DeWerd, L. A., Hanson, W. F., Saiful Huq, M., Ibbott, G. S., Mitch, M. G., Nath, R. & Williamson, J. F. (2004). Update of AAPM Task Group No. 43 Report: A revised AAPM protocol for brachytherapy dose calculations, *Medical Physics* **31**(3): 633–674.
- Rivard, M. J., Davis, S. D., DeWerd, L. A., Rusch, T. W. & Axelrod, S. (2006). Calculated and measured brachytherapy dosimetry parameters in water for the Xofigo X-Ray Source: An electronic brachytherapy source, *Medical Physics* **33**(11): 4020–4032.
- Schneider, T., Radeck, D. & Šolc, J. (2016). Development of a new primary standard for the realization of the absorbed dose to water for electronic brachytherapy x-ray sources, *Brachytherapy* **15**: S27–S28.
- Sechopoulos, I., Rogers, D. W., Bazalova-Carter, M., Bolch, W. E., Heath, E. C., McNitt-Gray, M. F., Sempau, J. & Williamson, J. F. (2018). RECORDS: improved reporting of monte Carlo Radiation transport studies: report of the AAPM Research Committee Task Group 268, *Medical physics* **45**(1): e1–e5.

1  
2  
3 *TG-43 parameters for the INTRABEAM source with spherical applicators* 26

- 4  
5 Seltzer, S. M., O'Brien, M. & Mitch, M. G. (2014). New national air-kerma standard for low-energy  
6 electronic brachytherapy sources, *Journal of research of the National Institute of Standards and*  
7 *Technology* **119**: 554–574.
- 8 Shaikh, M. Y., Burmeister, J., Scott, R., Kumaraswamy, L. K., Nalichowski, A. & Joiner, M. C.  
9 (2020). Dosimetric evaluation of incorporating the revised V4.0 calibration protocol for breast  
10 intraoperative radiotherapy with the INTRABEAM system, *Journal of applied clinical medical*  
11 *physics* **21**(2): 50–59.
- 12 Shamsabadi, R., Baghani, H. R., Azadegan, B. & Mowlavi, A. A. (2020). Monte Carlo based  
13 analysis and evaluation of energy spectrum for low-kV IORT spherical applicators, *Zeitschrift*  
14 *für Medizinische Physik* **30**(1): 60–69.
- 15 Vaidya, J. S., Wenz, F., Bulsara, M., Tobias, J. S., Joseph, D. J., Keshtgar, M., Flyger, H. L., Massarut,  
16 S., Alvarado, M. & Saunders, C. e. a. (2014). Risk-adapted targeted intraoperative radiotherapy  
17 versus whole-breast radiotherapy for breast cancer: 5-year results for local control and overall  
18 survival from the TARGIT-A randomised trial, *The Lancet* **383**(9917): 603–613.
- 19 Watson, P. (2019). *Dosimetry of a Miniature X-ray Source Used in Intraoperative Radiation Therapy*,  
20 PhD thesis, McGill University Libraries.
- 21 Watson, P. G. F., Bekerat, H., Papaconstadopoulos, P., Davis, S. & Seuntjens, J. (2018). An  
22 investigation into the INTRABEAM miniature x-ray source dosimetry using ionization chamber  
23 and radiochromic film measurements, *Medical Physics* **45**(9): 4274–4286.
- 24 Watson, P. G. F., Popovic, M. & Seuntjens, J. (2017). Determination of absorbed dose to water from a  
25 miniature kilovoltage x-ray source using a parallel-plate ionization chamber, *Physics in Medicine*  
26 *& Biology* **63**(1): 015016.
- 27 Watson, P. G. & Seuntjens, J. (2016). Effect of explicit M and N-shell atomic transitions on a low-  
28 energy x-ray source, *Medical physics* **43**(4): 1760–1763.
- 29 Yanch, J. C. & Harte, K. J. (1996). Monte Carlo simulation of a miniature, radiosurgery x-ray tube  
30 using the ITS 3.0 coupled electron-photon transport code, *Medical Physics* **23**(9): 1551–1558.
- 31  
32  
33  
34  
35  
36  
37  
38  
39  
40  
41  
42  
43  
44  
45  
46  
47  
48  
49  
50  
51  
52  
53  
54  
55  
56  
57  
58  
59  
60